Annals of Nuclear Medicine Vol. 16, No. 4, 255–261, 2002

# Correction of nonuniform attenuation and image fusion in SPECT imaging by means of separate X-ray CT

Toru KASHIWAGI,* Kenji YUTANI,* Minoru FUKUCHI,* Hitoshi NARUSE,** Tadaaki IWASAKI,** Koichi YOKOZUKA,*** Shinichi INOUE*** and Shoji KONDO***

**Department of Nuclear Medicine, Hyogo College of Medicine*
***Department of Cardiology, Hyogo College of Medicine*
****Hitachi Medical Corporation*

Improvements in image quality and quantitation measurement, and the addition of detailed anatomical structures are important topics for single-photon emission tomography (SPECT). The goal of this study was to develop a practical system enabling both nonuniform attenuation correction and image fusion of SPECT images by means of high-performance X-ray computed tomography (CT). A SPECT system and a helical X-ray CT system were placed next to each other and linked with Ethernet. To avoid positional differences between the SPECT and X-ray CT studies, identical flat patient tables were used for both scans; body distortion was minimized with laser beams from the upper and lateral directions to detect the position of the skin surface. For the raw projection data of SPECT, a scatter correction was performed with the triple energy window method. Image fusion of the X-ray CT and SPECT images was performed automatically by auto-registration of fiducial markers attached to the skin surface. After registration of the X-ray CT and SPECT images, an X-ray CT-derived attenuation map was created with the calibration curve for $^{99m}$Tc. The SPECT images were then reconstructed with scatter and attenuation correction by means of a maximum likelihood expectation maximization algorithm. This system was evaluated in torso and cylindlical phantoms and in 4 patients referred for myocardial SPECT imaging with Tc-99m tetrofosmin. In the torso phantom study, the SPECT and X-ray CT images overlapped exactly on the computer display. After scatter and attenuation correction, the artifactual activity reduction in the inferior wall of the myocardium improved. Conversely, the incresed activity around the torso surface and the lungs was reduced. In the abdomen, the liver activity, which was originally uniform, had recovered after scatter and attenuation correction processing. The clinical study also showed good overlapping of cardiac and skin surface outlines on the fused SPECT and X-ray CT images. The effectiveness of the scatter and attenuation correction process was similar to that observed in the phantom study. Because the total time required for computer processing was less than 10 minutes, this method of attenuation correction and image fusion for SPECT images is expected to become popular in clinical practice.

**Key words:** nonuniform attenuation correction, image fusion, image registration, single-photon emission tomography, X-ray computed tomography

## INTRODUCTION

SINGLE-PHOTON EMISSION TOMOGRAPHY (SPECT) is used extensively in diagnostic nuclear medicine for qualitatively and quantitatively assessing radiopharmaceutical distribution *in vivo*. A major limitation of both qualitative and quantitative SPECT is inaccuracy due to incorrect compensation for attenuated photons.

Received January 30, 2002, revision accepted April 12, 2002.
For reprint contact: Toru Kashiwagi, M.D., Department of Nuclear Medicine, Hyogo College of Medicine, 1–1 Mukogawa-cho, Nishinomiya, Hyogo 663–8501, JAPAN.
E-mail: kashiwag@hyo-med.ac.jp

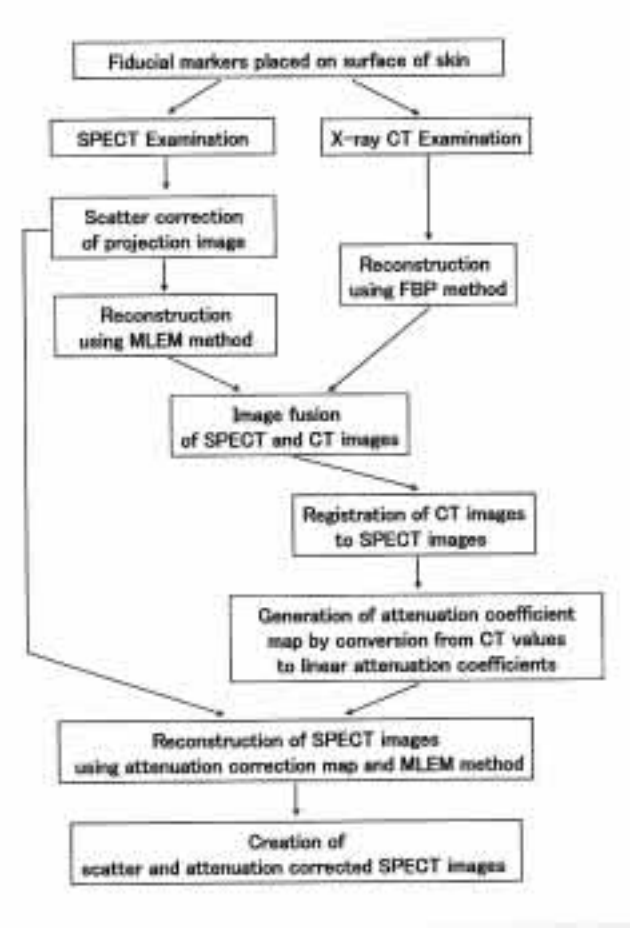


**Fig. 1** Flow-chart of scatter and attenuation correction for SPECT imaging using separate X-ray CT image.

Several methods of nonuniform attenuation correction (NUAC) for SPECT images by means of sequential or simultaneous transmission scans with an external source such as $^{99m}$Tc, $^{241}$Am or $^{153}$Gd have been reported[1–9] and are commercially available, but the clinical usefulness of these methods remains debatable. On the other hand, the utilization of X-ray computed tomography (CT) data for attenuation correction has been proposed since the end of the 1980s.[10–13] This method is not widely used in clinics and little information about its validity is available. A combined system consisting of X-ray CT and SPECT or positron emission tomography (PET) has recently been developed[14–16] and is expected to contribute greatly to precise understanding of the anatomical and functional states of diseased organs and the quantification of SPECT images by NUAC, but integrated X-ray CT is not high-performance and image quality is not sufficient for precise anatomical diagnosis.[14] Even if a high-performance X-ray CT is combined with SPECT, the examination throughput of the combined systems is usually not very high. The X-ray CT cannot be used to examine other patients whenever a SPECT examination is being performed. The examination times required for high-performance X-ray CT and SPECT are very different, the former requiring only a few minutes and the latter usually requiring about 30 minutes. Furthermore, a SPECT apparatus is not usually used for a SPECT study requiring an additional X-ray CT examination. Therefore, more suitable systems are needed for clinical use. Such a demand can now be reasonably met, since computer technology, such as image processing and networking, has made rapid progress in recent years. In view of these advances, we felt that the use of a separate X-ray CT system for SPECT NUAC should be reevaluated.

The goal of this study was to develop a practical system enabling both NUAC and image fusion of SPECT images with a separate high-performance X-ray CT system. The performance of this system was then evaluated in phantom and patient torso studies. Preliminary accounts of this work have appeared elsewhere.[17]

## MATERIALS AND METHODS

A SPECT/PET system (Forte, ADAC Laboratories, Milpitas, CA) and a helical X-ray CT scanner (Prima, Hitachi Medical Co., Tokyo) were used in the study. The systems were placed adjacent to each other and linked by Ethernet. To avoid positional differences between the SPECT and X-ray CT studies, identical flat patient tables were prepared for the two scanners. Body distortions were adjusted for by applying a laser beam to the skin surface from the upper and lateral directions. A cylindrical acrylic tube (inner diamter: 4 mm, length: 15 mm) containing an aqueous solution of $^{99m}$Tc and a contrast medium was used as a fiducial marker. These markers were attached to the skin surface to obtain precise registration of both images. Typically, 4 or 5 markers were used. The two scans were performed sequentially.

SPECT acquisition was performed with a noncircular orbit by means of dual detectors equipped with a low-energy, high-resolution collimator. One hundred and twenty-eight projections were acquired over 360° with 3 energy windows (140 keV ± 10%, 122 keV ± 2.5%, 158 keV ± 2.5%). Projection data were collected for 15 seconds per view and into a 64 × 64 matrix with 5.9 mm pixels.

The CT examination (120 kVp, 50 mAs, 1.0-second scanning time, 7-mm section thickness) was performed in the helical mode with a table speed of 5-mm per second. Reconstruction was performed by means of a standard reconstruction algorithm and a 512 × 512 matrix with a 0.74 mm pixel. The patients were asked to breathe shallowly during the scanning period.

The scatter and attenuation correction software was developed on a Pegasys workstation (ADAC Laboratories, Milpitas, CA). A flowchart describing the process is shown in Figure 1. For the projection of raw SPECT data, scatter correction was performed by a triple energy window (TEW) method.[18] The reconstruction was performed by means of a maximum likelihood expectation

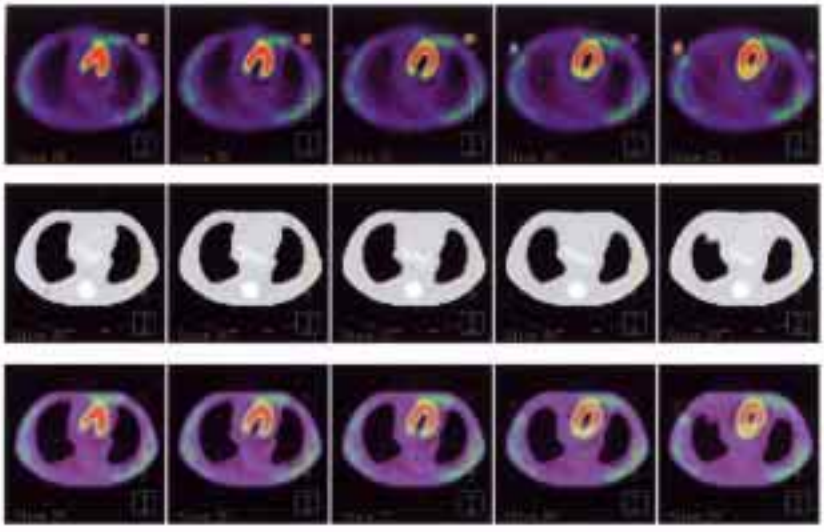

**Fig. 2** Torso phantom, uncorrected SPECT transverse images (*upper row*), X-ray CT derived attenuation map (*middle row*), and overlapping X-ray CT and SPECT images (*bottom row*).

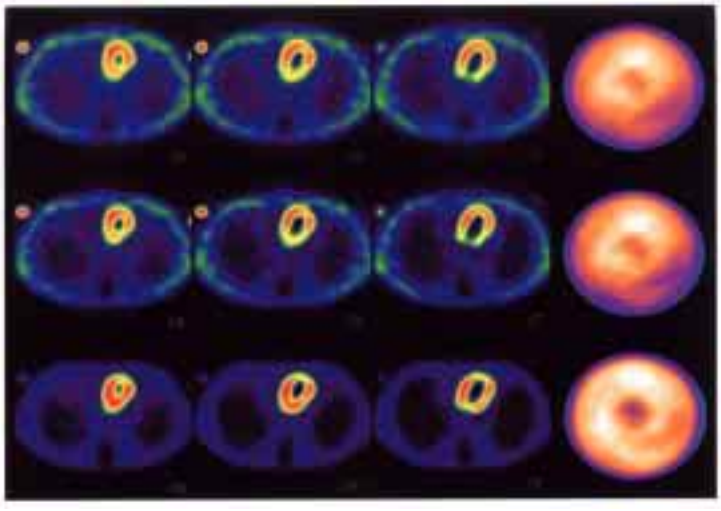

**Fig. 3** Transverse images and myocardial polar maps of the thorax of a torso phantom. The images are uncorrected (*upper row*), corrected for scatter and uncorrected for attenuation (*middle row*), and corrected for both scatter and attenuation (*bottom row*). Polar maps are shown to the right.

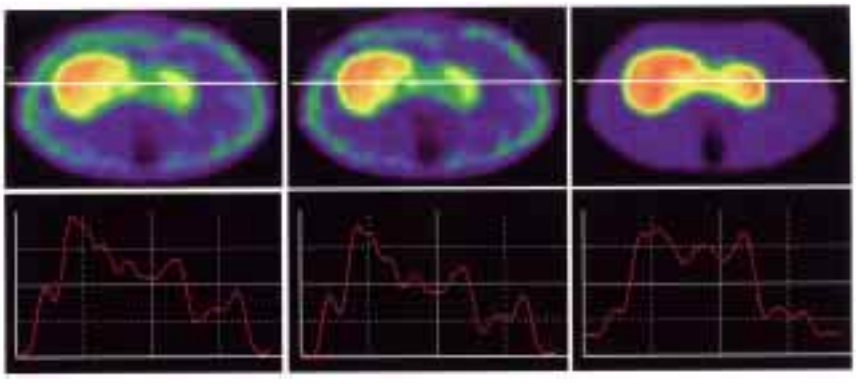

**Fig. 4** Transverse images of the abdomen of a torso phantom. The images are uncorrected (*upper left*), corrected for scatter and uncorrected for attenuation (*upper middle*), and corrected for both scatter and attenuation (*upper right*). Profile curves are shown at the bottom.

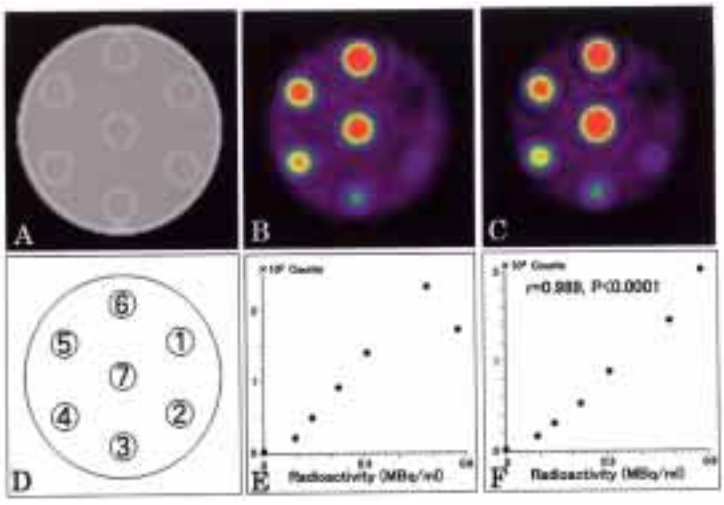


**Fig. 5** CT image (A) and SPECT images before (B) and after (C) scatter and attenuation correction of a circular cylinder phantom containing 7 small cylinders with different radioactivity levels. D shows a diagram of the phantom. The relationship between radioactivity counts on the SPECT image and the true radioactivity levels within the cylinders is shown before (E) and after (F) scatter and attenuation correction.

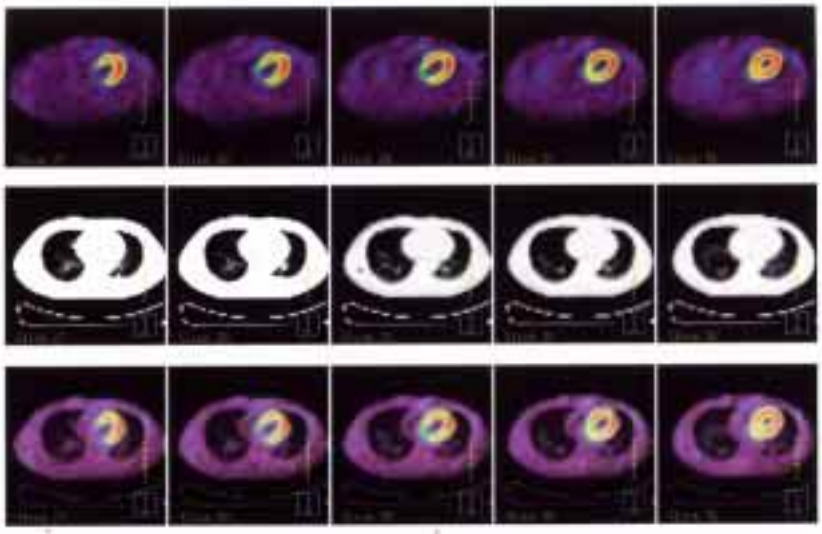

**Fig. 6** SPECT images of a patient after the intravenous injection of $^{99m}$Tc-tetrofosmin. Uncorrected SPECT transverse images (*upper row*), X-ray CT derived attenuation map (*middle row*), and overlapping image of X-ray CT and SPECT images (*bottom row*).

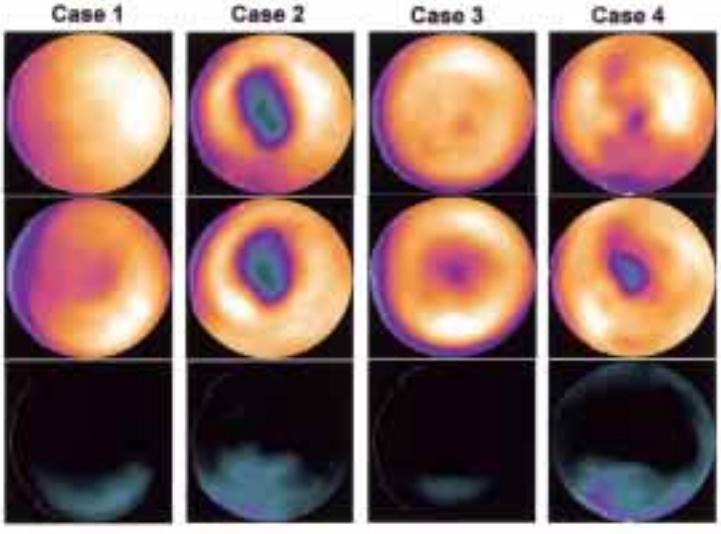


**Fig. 7** Two-dimensional polar maps of myocardial perfusion SPECT in 4 patients with heart disease. The images are uncorrected (*upper row*), corrected for scatter and attenuation (*middle row*), and the difference between uncorrected and corrected images (*bottom row*).

maximization (MLEM) algorithm.[19] X-ray CT slice data were retrieved from the X-ray CT workstation via DICOM. CT slices were then converted to a SPECT-like data volume (5.9 mm × 5.9 mm × 5.9 mm) for image fusion of the CT and SPECT images. Image fusion was automatically performed with computer software that made the CT and SPECT data sets match by minimizing the distance between the centroids of corresponding markers in the two images.[20] Finally, the validity of the image fusion was evaluated on the computer display. After the CT images were registered with the SPECT images, the CT number was converted to the linear attenuation coefficient ($\mu$) of $^{99m}$Tc (140 keV). The following equations (1 and 2) were used for the relationship between CT number and $\mu$ (/cm), based on experimental studies and theoretical calculations.

$$\mu = 0.152 \times (CT + 1000)/1000 \qquad CT \leqq 0 \quad (1)$$

$$\mu = 0.020 \times (CT + 1000)/1000 + 0.132 \qquad CT > 0 \quad (2)$$

With this attenuation coefficient map and scatter-corrected projection data, the scatter and attenuation-corrected SPECT images were created by a MLEM method.

This system was evaluated with phantoms and patients. Phantom studies were performed on an anthropomorphic torso phantom with a cardiac insert (Data Spectrum, Chapel Hill, NC) and a circular cylindrical phantom (ANZAI Medical, Tokyo).

In the torso phantom, the lung was composed of a mixture of water and polystyrene foam beams. $^{99m}TcO_4^-$ was distributed in the water of the myocardium, liver and background regions with concentrations of 0.5 MBq/m*l*, 0.2 MBq/m*l* and 0.07 MBq/m*l*, respectively. In a large circular cylindrical phantom (diameter: 22 cm), $^{99m}TcO_4^-$ was distributed in the water within 6 small cylinders (diameter: 30 mm) and outside the cylinders. One small cylinder (No. 1) contained only water. The concentrations in the remaining cylinders and background were 0.1 MBq/m*l* (No. 2), 0.15 MBq/m*l* (No. 3), 0.22 MBq/m*l* (No. 4), 0.30 MBq/m*l* (No. 5), 0.50 MBq/m*l* (No. 6), 0.60 MBq/m*l* (No. 7) and 0.03 MBq/m*l* (background).

Patient studies were performed in 4 patients referred to us for myocardial perfusion imaging. Informed consent was obtained from all patients. The patients received 740 MBq of $^{99m}$Tc-tetrofosmin intravenously. Thirty minutes after the injection, SPECT and X-ray CT examinations were performed one after another.

The scatter and attenuation-corrected SPECT images were compared with ordinary SPECT images reconstructed by the same MLEM method. In a cylindrical phantom study, the relations between the counts and the radioactive concentrations in small cylinders were examined in the attenuation-uncorrected and -corrected SPECT images. The small circular region of interest (diameter: 3 pixels, 16.4 mm) was placed on the center of small cylinder SPECT image and the mean count of pixels was determined.

## RESULTS

*Phantom study*

Figure 2 shows the uncorrected thoracic transverse SPECT images, the attenuation coefficient maps and the exactly overlapping SPECT and X-ray CT images obtained in the torso phantom study. Figure 3 shows the SPECT images and the myocardial polar maps before and after the scatter and nonuniform attenuation correction process. A slight improvement in image contrast was observed after the scatter correction. By adding the NUAC, the artifactual activity reduction in the inferior and infero-septal walls of the myocardium was improved and apical reduction was visualized more clearly. Conversely, the increased activity around the torso surface and lung areas was decreased. Figure 4 shows the abdominal SPECT transverse images and profile curves before and after the scatter and attenuation correction process. The liver and background activity, which was originally uniform, again became uniform after the NUAC.

Figure 5 shows the result of the cylindrical phantom study. The counts of the centers of the cylinders were recovered after the NUAC, and a distinct linear relationship was observed between the counts on the SPECT images and the true radioactivity within the small cylinders ($r = 0.987$, $p < 0.001$).

*Clinical study*

Figure 6 shows the uncorrected SPECT images, the attenuation coefficient maps, and the exactly overlapping SPECT and X-ray CT images obtained in a patient. The clinical study also showed a good overlapping of the cardiac and skin surface outlines on the fused SPECT and X-ray CT images. Figure 7 shows a summary of the clinical myocardial perfusion study results for 4 patients. The results of the correction process were similar to those observed in the phantom study. After NUAC, the activity in the inferior and infero-septal walls of the myocardium increased and the apical reduction became more clearly delineated.

*Computer processing*

After SPECT and X-ray CT image acquisition, the total computer processing time for the development of the scatter and attenuation-corrected image was less than 10 minutes. The most time-consuming process was the fusion of the images. Although this process was automated, confirmation and/or fine adjustments were performed on the computer display if necessary, requiring a few minutes. Other processes, such as reconstruction by the MLEM method, scatter correction and the creation of attenuation maps, required less than one minute.

## DISCUSSION

NUAC is an important issue for the improvement of

image quality and quantitation measurements in SPECT imaging. Methods for performing NUAC with transmission scans of an external source are available commercially, but this process is not yet widely used in clinical practice. One reason for this lack of popularization is that this process sometimes generates serious image artifacts. Patient motion, low-quality transmission scan images resulting from low photon flux, and the algorithms that are used, can cause inaccurate corrections. Other reasons include the additional expenses for software and hardware, and longer scan times. If an ordinary separate X-ray CT could be used for this purpose, several of these problems would be solved. Furthermore, the image quality of the transmission scan is undoubtedly improved. One major problem with the use of separate X-ray CT is the need to exactly match both images. Organs in the torso are supple and easily distorted, depending on posture. To solve this problem, several countermeasures were adopted in this study including posture adjustment by means of a laser beam and identical flat patient tables. Finally, the automated image fusion was performed with computer software that utilizes fiducial markers as guides. The results of this study are considered to be extremely satisfactory, as shown in the figures.

Compared to simultaneous transmission methods which employ external sources, the major advantage of X-ray CT is the ability to obtain high-quality anatomical and pathological images simultaneously. The fusion of SPECT and X-ray CT images is also an important subject in nuclear medicine. This system enables both NUAC and image fusion functions. The pathological information obtained simultaneously from the X-ray CT may compensate for the additional radiation exposure. A combined X-ray CT and SPECT system is certainly close to the ideal imaging system. Nevertheless, with regard to the efficient utilization of high-performance X-ray CT equipment, combined systems are often inefficient in their use of X-ray CT scanner time. In our system, several SPECT or PET apparatuses can share one high-performance X-ray CT for NUAC and image fusion, and independent imaging diagnosis with X-ray CT alone is also possible.

The conversion from X-ray CT values to the attenuation coefficient of $\gamma$-rays is complicated because the energy spectrum of $\gamma$-rays is finite, whereas X-rays are continuous. The conversion equations used in previous reports often differed; in this study, the conversion equation was determined by means of narrow beam experiments and by referring to other reports.[10–13] As a result, attenuation correction was successfully achieved qualitatively and quantitatively, as shown in the figures. In particular, the successful quantification of radiation counts on the SPECT images may have a large impact on the accurate evaluation of the functional states of normal and diseased organs.

The additional time required for computer processing, including iterative reconstruction, scatter and attenuation correction, and image fusion, is relatively short. Although the most time-consuming process is image fusion, the fused image provides valuable precise anatomical-functional correlations. Furthermore, the quality of the anatomical image is much greater than that of images obtained with transmission scan and external sources.

The combined SPECT and X-ray CT imaging system described in this report appears to be clinically practical and potentially useful for attenuation correction and the image fusion of SPECT and X-ray CT images of the entire body. Further investigations on the application of this system to PET imaging are planned.

## ACKNOWLEDGMENTS

The authors thank Mr. Hitoaki Kitani, Ms. Etsuko Morishita, Ms. Sanae Yanoo, Mr. Yoshihiro Maeda, Mr. Kouichi Onoe and Mr. Keizo Tachibana for their technical assistance.

## REFERENCES

1. Malko JA, Heertum RLV, Gullberg GT, Kowalsky WP. SPECT liver imaging using an iterative attenuation correction algorithm and an external flood source. *J Nucl Med* 1986; 27: 701–705.
2. Bailey DL, Hutton BF, Walker PJ. Improved SPECT using simultaneous emission and transmission tomography. *J Nucl Med* 1987; 28: 844–851.
3. Manglos SH, Bassano DA, Thomas D, Grossman ZD. Imaging of the human torso using cone-beam transmission CT implemented on a rotating gamma camera. *J Nucl Med* 1992; 33: 150–156.
4. Galt JR, Cullom SJ, Garcia EV. SPECT quantification: a simplified method of attenuation and scatter correction for cardiac imaging. *J Nucl Med* 1992; 33: 2232–2237.
5. Frey EC, Tsui BMW, Perry JR. Simultaneous acquisition of emission and transmission data for improved thallium-201 cardiac SPECT imaging using a technetium-99m transmission source. *J Nucl Med* 1992; 33: 2238–2245.
6. Jaszczak RJ, Gilland DR, Hanson MW, Jang S, Greer KL, Coleman RE. Fast transmission CT for determining attenuation maps using a collimated line source, rotatable air-copper-lead attenuators and fan-beam collimation. *J Nucl Med* 1993; 34: 1577–1586.
7. Tan P, Bailey DL, Meikle SR, Eberl S, Fulton RR, Hutton B. A scanning line source for simultaneous emission and transmission measurements in SPECT. *J Nucl Med* 1993; 34: 1752–1760.
8. Ficaro EP, Fessler JA, Ackermann RJ, Rogers WL, Corbett JR, Schwaiger M. Simultaneous transmission-emission thallium-201 cardiac SPECT: effect of attenuation correction on myocardial tracer distribution. *J Nucl Med* 1995; 36: 921–931.
9. Celler A, Sitek A, Stoub E, Hawman P, Harrop R, Lyster D. Multiple line source array for SPECT transmission scans: simulation, phantom and patient studies. *J Nucl Med* 1998; 39: 2183–2189.
10. Fleming JS. A technique for using CT images in attenuation correction and quantification in SPECT. *Nucl Med Commun*

1989; 10: 83–97.
11. Damen EMF, Muller SH, Boersma LJ, Boer RW, Lebesque JV. Quantifying local lung perfusion and ventilation using correlated SPECT and CT data. *J Nucl Med* 1994; 35: 784–792.
12. Koral KF, Zasadny KR, Kessler ML, Luo JQ, Buchbinder SF, Kaminski MS, et al. CT-SPECT fusion plus conjugate views for determining dosimetry in iodine-131-monoclonal antibody therapy of lymphoma patients. *J Nucl Med* 1994; 35: 1714–1720.
13. Blankespoor SC, Wu X, Kalki K, Brown JK, Tang HR, Cann CE, et al. Attenuation correction of SPECT using X-ray CT on an emission-transmission CT system: myocardial perfusion assessment. *IEEE Trans Nucl Sci* 1996; 43: 2263–2274.
14. Bocher M, Balan A, Krausz Y, Shrem Y, Lonn A, Wilk M, et al. Gamma camera-mounted anatomical X-ray tomography: technology, system characteristics and first images. *Eur J Nucl Med* 2000; 27: 619–627.
15. Patton JA, Delbeke D, Sandler MP. Image fusion using an integrated, dual-head coincidence camera with X-ray tube-based attenuation maps. *J Nucl Med* 2000; 41: 1364–1368.
16. Beyer T, Townsend DW, Brun T, Kinahan PE, Charron M, Roddy R, et al. A combined PET/CT scanner for clinical oncology. *J Nucl Med* 2000; 41: 1369–1379.
17. Kashiwagi T, Yutani K, Fukuchi M, Naruse H, Iwasaki T, Yokozuka K, et al. Attenuation correction and image fusion of SPECT using separate X-ray CT. *J Nucl Med* 2001; 42 (Suppl): 197P.
18. Ogawa K, Harada Y, Ichihara T, Kubo A, Hashimoto S. A practical method for position dependent Compton-scatter correction in single photon emission CT. *IEEE Trans Med Imag* 1991; 10: 408–412.
19. Shepp LA, Vardi Y. Maximum likelihood reconstruction for emission tomography. *IEEE Trans Med Imag* 1982; MI-1; 113–122.
20. Nelder JA, Mead R. A simplex method for function minimization. *Computer J* 1965; 7: 308–313.